Analysis of the magnetoresistance contributions in a nanocrystallized Cr-doped FINEMET alloy

- L.F. Kiss[a], V. Franco[b], M. Csontos[c], L. Péter[a], C.F. Conde[b], A. Conde[b], T. Kemény[a], J. Tóth[a], L.K. Varga[a], I. Bakonyi[a,]

- [a] Research Institute for Solid State Physics and Optics, Hungarian Academy of Sciences, H-1525 Budapest, P.O. Box 49, Hungary
- [b] Departamento de Física de la Materia Condensada, Instituto de Ciencia de Materiales C.S.I.C., Universidad de Sevilla, Apartado 1065, 41080 Sevilla, Spain
- [c] Department of Physics, Institute of Physics, Budapest University of Technology and Economics and Research Group of the Hungarian Academy of Sciences, H-1111 Budapest, Budafoki út 6-8, Hungary

Abstract

The magnetoresistance (MR) was measured at 200, 250 and 300 K in magnetic fields up to B=12 T for a nanocrystallized $Fe_{63.5}Cr_{10}Nb_3Cu_1Si_{13.5}B_9$ alloy. Both the longitudinal (LMR) and transverse (TMR) component of the magnetoresistance decreased from B=0 to about 0.1 T. This could be ascribed to a giant MR (GMR) effect due to spin-dependent scattering of conduction electrons along their path between two Fe–Si nanograins via the non-magnetic matrix. Such a scattering may occur if the nanograin moments are not or only weakly coupled in the absence of a strong exchange coupling (due to the high Cr content in the matrix) and/or only weak dipole–dipole coupling is present (due to sufficiently large separations between the nanograins). For larger fields, the GMR saturated and a slightly nonlinear increase in MR with B was observed due to a contribution by the residual amorphous matrix. The anisotropic MR effect (AMR≡LMR−TMR) was negative for all fields and temperatures investigated. By measuring the MR of melt-quenched $Fe_{100-x}Si_x$ solid solutions with x=15, 18, 20, 25 and 28, the observed AMR could be identified as originating from the Fe–Si nanograins having a $D0_3$ structure.

Research Highlights

► Magnetoresistance (MR) of nanocrystallized $Fe_{63.5}Cr_{10}Nb_3Cu_1Si_{13.5}B_9$ up to 12 T. ► Small GMR effect due to non-aligned neighbouring Fe–Si nanograins. ► For large fields, slightly nonlinear MR due to the residual amorphous matrix. ► Negative AMR of the Fe–Si nanograins exhibiting the $D0_3$ structure. ► Negative AMR reported on melt-quenched $Fe_{100-x}Si_x$ solid solutions ($15 \leq x \leq 28$).

Keywords

- Magnetoresistance; Amorphous alloys; Nanocrystallization; FINEMET alloys; Fe–Si alloys

1. Introduction

Due to their extremely good soft magnetic properties, there has been a long-standing interest in FINEMET type nanocrystalline/amorphous composites [1]. Starting from an amorphous precursor of the composition $Fe_{73.5}Nb_3Cu_1Si_{13.5}B_9$, an appropriate heat-treatment causes a partial crystallization [1] during which ferromagnetic (FM) Fe–Si precipitates with grain sizes in the nanoscale regime appear in a residual amorphous matrix. The chemical composition of

these nanograins is in the range of 15–22 at% Si, and these precipitates exhibit an off-stoichiometric $D0_3$ structure [2] (the stoichiometric form is the Fe_3Si compound). Above the Curie point (T_c) of the amorphous matrix, i.e., in its paramagnetic (PM) state, the exchange coupling between the magnetic nanograins is strongly reduced and, at sufficiently high temperatures, the Fe–Si nanograins exhibit a superparamagnetic (SPM) behaviour [2].

Systems consisting of SPM particles embedded in a non-magnetic metallic matrix are called granular magnetic alloys. It has been found in some granular metals, e.g. Cu(Co) or Ag(Fe) [3] that, depending on the size and separation of the nanograins, there may be an interaction between their magnetizations. Such an interaction may arise due to a dipole–dipole coupling between the nanograin magnetic moments. As a result of this coupling, there will be a correlation between the orientation of the magnetic moments of the individual nanograins. Owing to this correlation, the apparent magnetic moment derived from the usual Langevin fit of the field dependence of the magnetization of an SPM assembly can strongly deviate from the actual individual cluster moment size. It has been demonstrated [4] and [5] that a FM coupling between precipitated nanograins may exist also in FINEMET type nanocomposites well above the Curie point of the residual amorphous matrix. At high temperatures, this coupling arises mainly from a dipolar interaction between the nanograin magnetic moments. Around the Curie point of the matrix, with increase in temperature a continuously diminishing exchange interaction mediated by the matrix conduction electrons may still exist [2].

It has been reported [6] and [7] that granular metals can exhibit the phenomenon of giant magnetoresistance (GMR) if the size of the SPM nanograins and the spacing between them is in an appropriate nanoscale range. Therefore, one might attempt to observe a GMR effect also in FINEMET type nanocrystallized alloys above the Curie point of the matrix. The magnetoresistance measurements may eventually yield also useful complementary information on the degree of coupling between magnetic nanograins and can perhaps shed some light on the origin of the interaction.

Whereas the magnetoresistance (MR) characteristics of amorphous alloys have been extensively investigated in the past, e.g., for the Fe–P [8], Fe–B [9], (Fe–Ni)–(B–P) [10], Fe–Cr–B [11], Fe–Cr–B–Si [12] and Fe–B–Si [13] systems and for two FINEMET type amorphous precursors [14] and [15], relatively few studies have been devoted to nanocrystallized alloys. Such investigations remained restricted to a Fe–Si–B alloy [13], two FINEMET type alloys [14] and [15], a Fe–Cu–V–Si–B alloy [16] as well as some Fe–Zr–Cu and Fe–Zr–Cu–Ru [17] alloys. It was only the last alloy system (Fe–Zr–Cu–Ru) in which the composition was taylored in a manner (by the addition of Ru) that MR measurements could be performed above the Curie point of the residual amorphous matrix. As expected, a clear GMR effect, albeit very small, could be observed after an appropriate nanocrystallization procedure [17].

It has been known [18] that replacing a small fraction of the Fe atoms by Cr atoms in FINEMET type alloys results in a significant decrease in the Curie temperature of the residual amorphous matrix of the nanocrystallized state. In some recent works, we have reported on the magnetic properties of an alloy of the composition $Fe_{63.5}Cr_{10}Cu_1Nb_3Si_{13.5}B_9$ both in the as-quenched state and in various stages of the nanocrystallization [4], [5], [19] and [20]. The addition of 10 at% Cr resulted in a Curie point at around room temperature for the as-quenched amorphous alloy [19] and [20]. Since in the nanocrystallized state the precipitated nanograins do not contain Cr, the residual amorphous matrix further enriches in Cr and, thus, its Curie point is expected to reduce down to even below room temperature.

The purpose of the present work was to investigate the MR behaviour in the vicinity of the Curie point of the residual amorphous matrix of a nanocrystallized $Fe_{63.5}Cr_{10}Cu_1Nb_3Si_{13.5}B_9$ alloy in order to reveal a possible GMR effect of the granular alloy type, similar to the previously reported case of a Fe–Zr–Cu–Ru alloy [17]. In order to better understand the MR features observed for our nanocrystallized alloy, the MR measurements have been extended also to a series of melt-quenched Fe–Si alloys with the $D0_3$ structure and having 15, 18, 20, 25 and 28 at% Si.

For the nanocrystallized alloy, at small magnetic fields, below about B=0.1–0.2 T, both the longitudinal and transverse MR components decreased with increase in B. This was ascribed to a GMR effect arising from the spin-dependent scattering of electrons for an electron path between two Fe–Si nanograins through a non-magnetic matrix (granular-type GMR). At larger fields, a slightly nonlinear increase in the MR was observed, which could be attributed to the residual amorphous matrix. The MR data obtained on the melt-quenched Fe–Si alloys enabled us to identify that the negative AMR effect observed in the nanocrystallized alloy originates from two consecutive electron scattering events within the same Fe–Si nanograin. The small saturation field (B_s≈0.1 T) of the GMR contribution indicated that though the Fe–Si nanograins are in a SPM state but due to their sufficiently large size their magnetic moments saturate at a relatively small field.

The paper is organized as follows. In Section 2, sample preparation and characterization details as well as measurement techniques are described. The experimental results for the magnetic and magnetoresistance behaviour of the samples with various structural states are described in Section 3. This is followed by a discussion of the individual magnetoresistance terms of the nanocrystallized $Fe_{63.5}Cr_{10}Cu_1Nb_3Si_{13.5}B_9$ alloy (Section 4) and a brief summary of the present results (Section 5).

2. Experimental

An alloy of the composition $Fe_{63.5}Cr_{10}Cu_1Nb_3Si_{13.5}B_9$ was prepared as a ribbon (∼10 mm wide and ∼25 μm thick) by melt-spinning. The nanocrystallized state was obtained by isochronally annealing the amorphous ribbon at 825 °C for 1 h in a halogen-lamp furnace in argon atmosphere [4]. X-ray diffraction (XRD) and transmission electron microscopy (TEM) measurements were used to establish the amorphous state of the as-quenched ribbon as well as to characterize the nanocrystallized state [4]. The same ribbons were used here as in our earlier works [4], [5] and [19]. The nanocrystallized $Fe_{63.5}Cr_{10}Cu_1Nb_3Si_{13.5}B_9$ alloy was shown [4] to consist of 12 nm $D0_3$ Fe–Si nanograins embedded in a residual amorphous matrix with an average separation of 7 nm between them (19 nm average distance between nanograin centers) and having a volume fraction of 20%. The Si content of the nanograins was about 15–25 at% [2] and the Curie temperature of this Fe–Si phase was around 900 K [21].

The rapidly quenched crystalline Fe–Si ribbons (∼1 mm wide and ∼20 μm thick) were also prepared by melt-spinning. An XRD study revealed a $D0_3$ structure in these ribbons [21] and their magnetic properties and zero-field electrical transport parameters have been reported elsewhere [21] and [22].

The magnetoresistance was measured by a four-point-in-line method on 1–2 mm wide strips, which were cut out of the ribbon pieces having a length of typically 5 mm for the Cr-containing samples and 15 mm for the Fe–Si alloys. A magnetic field of up to B=12 T was applied in two geometries in the ribbon plane: parallel and perpendicular to the current, which provided the longitudinal (LMR) and transverse (TMR) magnetoresistance, respectively. The MR was defined

by the relative change in the resistance (R) as a function of applied field, B, and was expressed as $\Delta R/R=[R(B)-R_0]/R_0$ where R_0 stands for the resistance in zero external magnetic field. The MR measurements were carried out by cycling the external magnetic field between the maximum field values.

The FM–PM transition of the nanocrystallized state of the $Fe_{63.5}Cr_{10}Cu_1Nb_3Si_{13.5}B_9$ alloy ribbon was studied by measuring the temperature dependence of the a.c. susceptibility in a home-made apparatus at 6 kHz frequency with an excitation field of B_{max}=2 μT.

3. Results

3.1. Nanocrystallized $Fe_{63.5}Cr_{10}Nb_3Cu_1Si_{13.5}B_9$ alloy

3.1.1. Temperature and field dependence of magnetoresistance

The experimental LMR and TMR data for the nanocrystallized state of the $Fe_{63.5}Cr_{10}Cu_1Nb_3Si_{13.5}B_9$ alloy at T=300 K are shown in Fig. 1a up to B=0.5 T and in Fig. 1b up to B=12 T, where the low-field data are also included. There is a good agreement between the two datasets as indicated in Fig. 1b when comparing the thick and thin lines representing the low-field and high-field data, respectively, for both the LMR and TMR components.

In the low-field data (Fig. 1a), one can see a small MR peak around B=0 for both the LMR and TMR components. The MR saturates for magnetic fields of about B=0.25 T after which a slightly nonlinear increase persisting up to 12 T (Fig. 1b) can be observed (the apparent asymmetry of the MR data, especially for the LMR component, is probably an instrumental artifact due to the very high sensitivity applied and the very long measurement time—during a full magnetic field cycle, typically 500–800 data points were recorded, which were then averaged over a certain range to achieve a sufficient signal-to-noise ratio).

Very similar magnetoresistance results were obtained also at T=250 (Fig. 2) and 200 K (Fig. 3).

At all three temperatures, both the LMR and the TMR components decrease first when increasing the magnetic field from B=0 up to a certain saturation field B_s that seems to decrease as the temperature is reduced (see Table 1). The identical sign of this initial change for both (LMR and TMR) components is indicative of a GMR effect caused by spin-dependent scattering of conduction electrons when travelling through a non-magnetic matrix between two magnetic regions in which the magnetization orientations are different from each other.

It can also be established from Fig. 1, Fig. 2 and Fig. 3 that the LMR and the TMR components are not equal to each other at all fields in the investigated temperature range. Beyond the saturation field, the difference is independent of the magnetic field. This behaviour is typical for the anisotropic magnetoresistance (AMR) of bulk homogeneous ferromagnets [23], [24] and [25] whereby the AMR is defined as the difference LMR−TMR. For the pure ferromagnetic metals (Fe, Co and Ni) as well as for most FM alloys, AMR>0, i.e., the LMR component is more positive than the TMR component.

In the present case, however, a negative AMR effect (AMR<0) can be observed (see Fig. 1, Fig. 2 and Fig. 3 and Table 1). Such a behaviour has already been reported previously for the nanocrystallized state of a $Fe_{78}B_{13}Si_9$[13], a $Fe_{72}V_3Cu_1Si_{16}B_8$[16] and two FINEMET type alloys [14] and [15]. On the other hand, in the amorphous state of Fe-based metal–metalloid alloys,

all reported magnetoresistance data [8], [9], [10], [11], [12], [13], [14], [15], [16] and [26] indicate a positive AMR and the same was found even for sputtered amorphous Fe–Si thin films [27] and [28]. Therefore, since in all the above listed nanocrystallized alloys as well as in our one, the FM grains consist of a Fe–Si alloy with the $D0_3$ structure, evidently these grains can be made responsible for the negative AMR effect observed in these nanocrystallized alloys. This has already been suggested [14] and [15] on the basis of old MR data on bulk Fe–Si alloys [29] and are supported also by MR results obtained more recently on crystallizing sputtered amorphous Fe–Si thin films [28]. All this also constituted a motivation for us to perform a more detailed study on the MR behaviour of rapidly quenched Fe–Si ribbons, and the results are presented in Section 3.2.

Another feature of the results presented above for the nanocrystallized $Fe_{63.5}Cr_{10}Cu_1Nb_3Si_{13.5}B_9$ alloy (see Figs. 1b, 2b and 3b) is the slightly nonlinear increase in the MR up to the highest magnetic fields investigated (B=12 T). Such a behaviour is typical for structurally disordered weak itinerant ferromagnets at temperatures around the FM–PM transition as demonstrated, e.g., for amorphous $Fe_{90-x}Mn_xZr_{10}$ ($0 \le x \le 16$) alloys [30]. An evaluation of the high-field MR data on our nanocrystallized $Fe_{63.5}Cr_{10}Cu_1Nb_3Si_{13.5}B_9$ alloy is presented in Section 4.3.

We have also measured the room-temperature MR of the as-quenched amorphous $Fe_{63.5}Cr_{10}Cu_1Nb_3Si_{13.5}B_9$ alloy up to B=0.2 T. In this field range, no measurable MR could be detected for either the TMR or the LMR components within an accuracy of at least 0.01%. This is in agreement with the facts that the Curie point of the as-quenched amorphous state is close to room temperature [19] and [20] and that the AMR may completely disappear in ferromagnetic alloys even somewhat below the Curie temperature [31].

3.1.2. Magnetic characterization of the nanocrystallized and amorphous states

The temperature dependence of χ_{ac} for the nanocrystallized $Fe_{63.5}Cr_{10}Cu_1Nb_3Si_{13.5}B_9$ alloy is shown in Fig. 4. Due to the high Curie point (about 900 K [21]) of the Fe–Si nanograins in the nanocrystallized $Fe_{63.5}Cr_{10}Cu_1Nb_3Si_{13.5}B_9$ alloy, the contribution of these nanograins to χ_{ac} is constant in the temperature range investigated (77–300 K). Therefore, the χ_{ac} data displayed in Fig. 4 reveal a FM–PM transition of the residual amorphous matrix. This observed magnetic transition is fairly broad, it spans actually the whole measurement temperature range. Nevertheless, it can be established that in the temperature range of the MR measurement from 200 to 300 K applied for the nanocrystallized alloy, the amorphous matrix has already mostly lost its FM state and is mainly paramagnetic. The rapid increase in the coercive field from 100 to 300 K reported for this alloy [5] indicates a loss of exchange softening, which provides evidence for the FM–PM transition of the residual amorphous matrix. This is further supported by the results of the Mössbauer measurements [4] according to which the residual amorphous matrix of a $Fe_{63.5}Cr_{10}Cu_1Nb_3Si_{13.5}B_9$ alloy nanocrystallized at 825 K for 1 h is definitely paramagnetic at room temperature.

3.2. Room-temperature magnetoresistance data on the melt-quenched Fe–Si alloys

The room-temperature MR curves for the melt-quenched Fe–Si ribbons with 18, 20, 25 and 28 at% Si were qualitatively very similar to each other for each composition studied. The experimental data for the selected $Fe_{80}Si_{20}$ alloy are presented in Fig. 5. For B>0.1 to 0.2 T, i.e., beyond technical saturation, both the LMR and TMR components linearly decreased with increase in magnetic field. Since the LMR component is more negative than the TMR component at all field values, we get the anisotropic magnetoresistance AMR=LMR–TMR<0 for each composition, i.e., these alloys exhibit a negative AMR, just as the nanocrystallized sample.

The evolution of the AMR magnitude and the slope of the linear high-field MR sections with Si content is summarized in Table 2 where the LMR and TMR values taken at B=0.8 T are also displayed. It should be noted that whereas the linearity of the MR data beyond technical saturation is well fulfilled for 20, 25 and 28 at% Si, both the LMR and TMR data tend to decrease more rapidly than linear in the same magnetic field range for the sample with 18 at% Si.

The transverse MR component exhibits a salient feature at low magnetic fields (Fig. 5b). The MR first decreases slightly when B increases from 0 and it starts to increase only after a small minimum. At technical saturation it then reaches a maximum before entering the linearly decreasing section. The minimum field and the MR value at the minima are also provided in Table 2. At present, the origin of this minimum is not clear.

The MR behaviour of the $Fe_{85}Si_{15}$ ribbon was rather inhomogeneous: ribbon pieces with either AMR<0 or AMR>0 were found whereby the magnitude of the AMR was around 0.1%. This may indicate that at this composition, the rapidly quenched ribbon, besides the phase with a $D0_3$ structure and having AMR<0, may also contain regions, where the bcc Fe–Si solid solution phase with AMR>0 appears and the fraction of the two phases fluctuates randomly along the ribbon length. It is noted that the relatively large error observed in the magnitude of the zero-field resistivity of this alloy ribbon [21] could also have been a consequence of its random two-phase nature.

4. Discussion

In the present paper, the main interest is focused on understanding the magnetoresistance behaviour of the nanocrystallized $Fe_{63.5}Cr_{10}Nb_3Cu_1Si_{13.5}B_9$ alloy. It appeared from Section 3 that the observed magnetoresistance may be considered to consist of three major contributions: (i) a GMR contribution due to the spin-dependent scattering of electrons travelling between the magnetic Fe–Si nanograins embedded in a more or less non-magnetic matrix, (ii) an AMR contribution arising from the interior of the Fe–Si nanograins and (iii) a high-field contribution attributable to the residual amorphous matrix having its magnetic transition temperature in the vicinity of the temperature of the MR measurements. In the following, we shall discuss these three major MR contributions by also exploiting supplementary magnetoresistance and magnetic data reported in Section 3 on the same alloy and on other related alloy samples.

4.1. Low-field MR contribution: granular-type GMR due to magnetic Fe–Si nanograins in a non-magnetic matrix

As Fig. 1, Fig. 2 and Fig. 3 demonstrate, in the temperature range from 200 to 300 K both the longitudinal and transverse MR components have the same sign (negative) for small magnetic fields. This indicates that the observed magnetoresistance in the low-field region can be ascribed to the GMR effect. The phenomenon of GMR can occur in metallic magnetic nanostructures, which consist of nanoscale magnetic entities separated by similarly nanoscaled non-magnetic regions (magnetic/non-magnetic multilayers or granular alloys containing small magnetic clusters embedded in a non-magnetic matrix). The separation of the magnetic entities should be small enough so that conduction electrons when polarized by the magnetization of one magnetic region can preserve this spin information till arriving at the next magnetic region. If a current-carrying electron travels through the non-magnetic matrix from magnetic region A to magnetic region B and the orientations of the magnetizations (magnetic moments) of these regions are different, the electron undergoes a so-called spin-

dependent scattering in region B. If the magnetization orientations of these regions are the same, no such spin-dependent scattering occurs. Therefore, in the latter case the resulting resistance will be definitely smaller than in the first case whereas the “background” resistance of non-magnetic origin remains the same in both cases. If the magnetization orientations of regions A and B are different in zero external magnetic field, then we can observe the GMR effect when aligning the two magnetizations parallel by a sufficiently large external magnetic field. The magnitude of the GMR effect is larger, the larger is the difference of the magnetization orientations between regions A and B in zero magnetic field.

According to the discussion in ‘Introduction’ and the magnetic data in Section 3.1.2, the nanocrystallized $Fe_{63.5}Cr_{10}Cu_1Nb_3Si_{13.5}B_9$ alloy consists of magnetic nanograins embedded in a residual amorphous matrix, which has a broad FM–PM transition just in the temperature range of the MR measurements. The low-field magnetoresistance data (Figs. 1a–3a) of this alloy show an initial decrease in the resistivity when increasing the magnetic field from B=0 for both the LMR and TMR components. This behaviour is qualitatively similar to that of a previously investigated nanocrystallized Fe–Zr–Cu–Ru [17] alloy and we can assign in both cases the observed resistivity change to a GMR effect. However, there are also differences in the MR behaviour of the two alloys, namely, whereas the MR curves for the Fe–Zr–Cu–Ru [17] alloy showed no saturation even in magnetic fields at least up to 1 T, the saturation fields of the MR components, which can be ascribed to a GMR effect in our alloy, are much smaller (see Fig. 1, Fig. 2 and Fig. 3 and Table 1). The large MR saturation fields for the Fe–Zr–Cu–Ru [17] alloy arise because in this case the precipitated superparamagnetic nanograins are small for which saturation can be achieved in very large magnetic fields only.

On the other hand, in our nanocrystallized $Fe_{63.5}Cr_{10}Cu_1Nb_3Si_{13.5}B_9$ alloy the situation seems to be different. From earlier studies [4], we know the size of the magnetic Fe–Si nanograins in our nanocrystallized alloy: the average diameter is 12 nm and the average magnetic moment is 112 000 μ_B. This relatively large moment leads to a much smaller saturation field (B_s≈0.1–0.2 T), which is comparable with the observed saturation fields of the MR components.

The magnetization direction of each individual nanograin is fixed by the crystal anisotropy and the exchange and/or dipolar interaction of the nanograins. In case the intergrain interactions are not very strong or partly destroyed by the sufficiently high temperature, the nanograin orientations can be random to some extent and this ensures that the magnetizations of two neighbouring regions will be with high probability in a non-aligned state in zero magnetic field. This configuration results in a larger resistivity in comparison with the case when the magnetic nanograins are all aligned along the magnetic field. This is an important pre-requisite for the occurrence of a GMR effect.

For the GMR effect, the resistance change is expected to be the same for any orientation of the external magnetic field and the measuring current, i.e., LMR should be equal to the TMR component, which is not the case for the nanocrystallized $Fe_{63.5}Cr_{10}Cu_1Nb_3Si_{13.5}B_9$ alloy (Fig. 1, Fig. 2 and Fig. 3). This is due to the presence of an AMR effect to be discussed in Section 4.2. To get the isotropic GMR from the measured LMR and TMR data, we follow the usual procedure [23] and [24] according to which, in the magnetically saturated state (B>B_s), the isotropic resistivity ρ_{is} is defined as

(1)

$$\rho_{is} \equiv (1/3)\rho_{Ls} + (2/3)\rho_{Ts}$$

Here, ρ_{Ls} and ρ_{Ts} are the resistivities of the longitudinal (L) and transverse (T) component, respectively, of the saturated state. In analogy, the saturation value of the isotropic GMR contribution can be obtained as

(2)

$GMR_s=(1/3)LMR_s+(2/3)TMR_s$

where LMR_s and TMR_s are the saturation values of the longitudinal and transverse components, respectively, which can be obtained by taking an average of the corresponding experimental data in the field range $B>B_s$.

The average saturation GMR_s values established in this manner from the experimental LMR and TMR components for $B>B_s$ for the nanocrystallized $Fe_{63.5}Cr_{10}Cu_1Nb_3Si_{13.5}B_9$ alloy are summarized in Table 1. It should be emphasized again that Eqs. (1) and (2) are valid only in the magnetically saturated state.

By looking at the experimental data in Figs. 1a, 2a and 3a, we can estimate an error of about 30% on the magnitude of the GMR (due to the uncertainty where to put the saturation resistivity on the noisy and in some cases asymmetric MR curves; the latter feature created owing to the electronic drift at the extremely high sensitivity that had to be applied as noticed in Section 3.1.1). In spite of the noisy character of the experimental data, their reliability can be further assessed from the fact that the separately recorded low-field and high-field MR data are nicely superimposed for all three temperatures (see Figs. 1b, 2b and 3b) and Fig. 2a also shows two independent sets of low-field data properly superimposed on each other.

Since we cannot be sure that the zero-field remanent state indeed corresponds to the maximum degree of antiparallel magnetization alignment of neighbouring magnetic regions (isotropic distribution of magnetic domain orientations), the reported GMR data represent a lower limit only. Thus, whereas the presence of a clear isotropic GMR is unambiguous, the actual GMR values can be higher than given here.

If we consider the data in Table 1, we can see that the observed GMR is very small. A comparison with the room-temperature data obtained by Suzuki et al. on the Fe–Zr–Cu–Ru alloy (see Fig. 3 of Ref. [17]) at our saturation field for 300 K (B_s=0.25 T) reveals that the GMR in the Fe–Zr–Cu–Ru alloy is about 0.025%, which is larger than our corresponding value by about a factor of 3. This larger GMR can be explained by the fact that in the Fe–Zr–Cu–Ru alloy the grains are much smaller (i.e., their density can be much higher); thus the occurrence of electron paths “FM nanograin → amorphous non-magnetic spacer → FM nanograin” is simply more abundant. The larger grain size in our sample is also consistent with our smaller saturation field as discussed at the beginning of this section.

The small value of the GMR can be caused by several factors. As noted above, though our GMR is smaller, it is still comparable to that of the Fe–Zr–Cu–Ru alloy in the same low field (our B_s value at 300 K). One important reason for the low GMR in these disordered nanocrystallized alloys is due to the high zero-field (background) resistivity, which can be 100 μΩ cm or more (see Ref. [17]) since this quantity appears in the denominator of the definition of the magnetoresistance: $MR=\Delta R/R$. In addition, the amorphous spacer regions between the FM nanograins have a very small mean free path for the conduction electrons (roughly equal to the atomic spacing). A long mean free path is essential for having a large GMR; this situation is realized in ferromagnetic/non-magnetic multilayers with pure non-magnetic metal spacers

and, then, the GMR decreases exponentially with spacer thickness. A partial collinearity of the neighbouring nanograin magnetizations (non-complete random alignment) can also be an important reason for the low GMR since we have no exact information on the residual coupling between nanograins and the non-collinearity can indeed be small under all conditions investigated. If this is indeed a significant factor for the low GMR, such a low level of non-collinearity can also be a sign for a significant exchange interaction between the nanograins. Although we do not have direct information about the strength of coupling between nanograins, the temperature evolution of experimental data can still give us useful hints. According to Section 3.1.2, although the FM–PM transition of the residual amorphous matrix (spacer material) is fairly broad in our nanocrystallized alloy, the amorphous matrix is already in the PM state at the highest temperature investigated (T=300 K). The saturation field values summarized in Table 1 (B_s strongly increases with increase in temperature) give further support to the picture that the nanograins are much more decoupled at 300 K (B_s=0.25 T) than at 200 K (B_s=0.01 T), speaking for a substantial reduction in the exchange coupling between nanograins over the temperature range investigated. In line with this, the GMR is reported to be −0.008% at 300 K and −0.005% at the two lower temperatures investigated. This can be accepted as a significant decrease (by almost a factor of 2) when entering the FM temperature range of the spacer even if it is hard to see this directly from the measured MR curves (Figs. 1a, 2a and 3a) owing to the fairly high (inverse) AMR component present due to the bulk behaviour of the Fe–Si nanograins as discussed in the next section.

4.2. AMR contribution of the ferromagnetic Fe–Si nanograins

As it was mentioned in Section 3.1.1, the MR data on the nanocrystallized $Fe_{63.5}Cr_{10}Cu_1Nb_3Si_{13.5}B_9$ alloy (Fig. 1, Fig. 2 and Fig. 3) indicated the presence of a negative AMR effect, i.e., AMR≡LMR–TMR<0. In line with this finding, the MR data on the melt-quenched Fe–Si alloys (Section 3.2 and Fig. 5) exhibited the same behaviour. This suggested to ascribe the observed negative AMR effect in the nanocrystallized alloy to the Fe–Si nanograin precipitates with the $D0_3$ structure in agreement with the former works [14] and [15].

Having established the isotropic saturation contribution GMR_s from the experimental data (Figs. 1a–3a), we can now trace out the individual magnetoresistance contributions due to the ferromagnetic Fe–Si nanograins, namely, the saturation value of the longitudinal magnetoresistance component of the Fe–Si nanograins can be obtained as

(3a)

$$LMR_s=LMR_s(Fe{-}Si)+GMR_s$$

and, similarly, for the transverse component we have

(3b)

$$TMR_s=TMR_s(Fe{-}Si)+GMR_s$$

where LMR_s and TMR_s correspond to the average saturation values ($B>B_s$) of the experimental data in Figs. 1a–3a as in Eq. (2). The average LMR_s(Fe–Si) and TMR_s(Fe–Si) values are also summarized in Table 1 for each temperature investigated. In contrast to the GMR, which is derived from an averaging of the LMR and TMR components, for the AMR the error can be larger (maybe 50%) since it derives from the difference of the LMR and TMR saturation values.

In this manner, the average saturation magnetoresistance data for $B>B_s$ in Table 1 represent the individual saturation contributions arising, on the one hand, from a GMR effect due to electron scattering events along a path connecting two neighbouring Fe–Si nanograins with non-aligned magnetization and, on the other hand, from electron scattering events within the FM Fe–Si nanograins (the bulk AMR effect).

An AMR effect arises if two consecutive electron scattering events occur within the same FM region, i.e., within the same Fe–Si nanograin. By using available structural and electrical transport data, we can make an estimate if such electron scattering events can happen in the nanocrystallized alloy. The electronic mean free path (ℓ_e) can be estimated by using the formula [32]:

(4)

$$\ell_e\,[\mathrm{nm}] = 9.2(r_s/a_o)^2/\rho[\mu\Omega\,\mathrm{cm}]$$

where a_o is the Bohr radius, ρ the resistivity and r_s the radius of an equivalent sphere ascribed to a conduction electron, which can be derived from the conduction electron density n via the relation $1/n=4\pi(r_s)^3/3$. The ratio r_s/a_o ranges [32] from 2 to 6 for all metals. By taking $r_s/a_o=4$ as the mean value, we may estimate the mean free path as $\ell_e[\mathrm{nm}]\approx 150/\rho$ [μΩ cm] (the uncertainty may amount to a factor of about 2). We will use the same expression for the Fe–Si nanograin material. According to Ref. [21], the room-temperature electrical resistivity of Fe–Si alloys with the $D0_3$ structure is about 100 μΩ cm for Si contents from 15 to 20 at%, which is just the concentration range of the Fe–Si nanograins [2]. Thus, we get that the electronic mean free path in the nanograins is about 1.5 nm (within a factor of 2). Since the average Fe–Si grain size is about 12 nm [4], this means that a conduction electron undergoes numerous consecutive scattering events within each nanograin, contributing to an AMR effect typical for the bulk Fe–Si material. This gives us a further justification for ascribing the AMR contribution observed in the nanocrystallized alloy to the Fe–Si nanograin phase.

We can also account for the fact that the magnitude of the AMR contribution due to the nanograins in the nanocrytallized alloy is apparently much smaller than the AMR of the melt-quenched Fe–Si ribbons with Si contents of 18 at% and above, namely, the nanograins are embedded in an amorphous matrix and the high background resistivity of the latter strongly reduces the magnitude of the measured magnetoresistance ratio and of its all components.

A further argument that the observed AMR component cannot arise from the residual amorphous matrix is that the AMR is expected to strongly reduce when the temperature rises close to the vicinity of the Curie point (and becomes actually zero above T_c) whereas our MR measurements were performed close to or above the Curie point of the amorphous matrix.

For characterizing the electrical transport in FM metals, it is customary [24], [25], [33] and [34] to introduce an asymmetry parameter $\alpha=\rho\downarrow/\rho\uparrow$ where $\rho\downarrow$ and $\rho\uparrow$ correspond, in terms of the two-current model of Mott [25] and [33], to the resistivities of the independent ↑ and ↓ conduction channels, respectively. On the other hand, it is also a basic feature of the Mott model [25], [33] and [34] that in d-band metals the carriers of the electrical current, mainly s-band electrons, can be scattered also into d-band states and the scattering probability is proportional to the density of d-band states $N_d(E_F)$ available as final states for the scattered s-electrons at the Fermi level E_F. This means that the main source of resistivity is the s–d scattering mechanism of conduction electrons. In this sense, we get that $\rho\downarrow\propto N_{d\downarrow}(E_F)$ and

$\rho\uparrow \propto N_{d\uparrow}(E_F)$. Since in d-band metals usually $N_d(E_F) >> N_s(E_F)$, the asymmetry parameter α can now be written as $\alpha = N_{d\downarrow}(E_F)/N_{d\uparrow}(E_F)$. For strong itinerant ferromagnets (SIF) in which the majority spin d↑-band is full and only minority spin d↓-band states are present at the Fermi level, we have, therefore, $N_{d\downarrow}(E_F) >> N_{d\uparrow}(E_F)$, i.e. $\alpha >> 1$. For SIF metals and alloys, theory predicts [34] that the AMR is positive and typically larger than +1%. For weak itinerant ferromagnets (WIF) for which both majority spin d↑-band and minority spin d↓-band states are present at E_F, $N_{d\downarrow}(E_F)$ and $N_{d\uparrow}(E_F)$ are typically comparable to each other and either of them can be larger than the other, i.e., both cases $\alpha > 1$ and $\alpha < 1$ may occur. Therefore, for WIF metals and alloys [34] if $\alpha > 1$, the AMR is predicted to be positive but its magnitude remains typically below +1% whereas for $\alpha < 1$, the AMR is negative and not exceeding −1%. These conclusions were based on considerations of electrical transport results on dilute ferromagnetic alloys and on such systems they were indeed found to be well obeyed by both the magnitude and the sign of the experimental AMR data [34].

It may be instructive to compare the AMR results and their interpretation for Ni-rich ferromagnetic Ni–Cu and Ni–Cr alloys. For the Ni–Cu system, the AMR is positive with a maximum of about +7% around 10 at% Cu at 4.2 K [35]. According to the band structure calculations of Vernes et al. [36], in the whole ferromagnetic regime $N(E_F)$ is dominated by the Ni minority band d↓ states and, therefore, $N_{d\downarrow}(E_F) >> N_{d\uparrow}(E_F)$ from which we get $\alpha >> 1$. In this way, the large observed positive AMR values are well explained on the basis of the two-current model of AMR [34]. For Ni–Cr alloys, the AMR is negative at low temperatures [37], [38] and [39], varying between −0.2% and −0.3% in the concentration range of 1–7 at% Cr [39]. It has already been suggested [39] that the negative AMR values in these Ni–Cr alloys are due to the presence of Cr virtual bound states at the Fermi level. Band structure calculations [36] have, indeed, revealed the presence of Cr d-band virtual bound states at the Fermi level in a way that $N\uparrow(E_F) > N\downarrow(E_F)$. This leads finally to $\rho\uparrow > \rho\downarrow$ and $\alpha < 1$, well explaining the occurrence of a negative AMR in this system on the basis of the model of Campbell et al. [34].

Unfortunately, this picture does not seem to be applicable for pure Fe metal and for Fe–Si alloys. The WIF character of body-centred cubic (bcc) Fe is well demonstrated by band structure calculations [40], [41] and [42] with $N\uparrow(E_F) > N\downarrow(E_F)$. The Fe_3Si compound with the $D0_3$ structure was also found to exhibit WIF behaviour by band structure calculations [42] and [43] and, here, it was obtained that $N\uparrow(E_F) < N\downarrow(E_F)$. (It should be noted that band structure calculations for disordered bcc-$Fe_{75}Si_{25}$ alloys [44] also indicated the relation $N\uparrow(E_F) < N\downarrow(E_F)$.) Therefore, according to the model of Campbell et al. [34], bcc-Fe is expected to have small negative AMR whereas experiments indicate small positive AMR [25] and [33]. On the other hand, $Fe_3Si(D0_3)$ is expected to have small positive AMR but, as we have shown above, this phase has a small negative AMR. Apparently, the currently available model [34] is not capable of accounting for the sign of AMR in bcc-Fe and in Fe–Si alloys; therefore, further theoretical work is needed to resolve this problem. The inadequacy of this model in its original form to certain alloy systems has already been pointed out by Banhart et al. [45].

4.3. High-field MR contribution of the residual amorphous matrix

In any metals, even if non-magnetic, there is a MR contribution due to the effect of a magnetic field on the electron motion [24] and [25] and this gives rise to a quadratic increase in the magnetoresistance with increase in magnetic field. Apparently, this contribution is negligible in the present nanocrystallized alloy since the data in Figs. 1b, 2b and 3b suggest a monotonic, slightly nonlinear increase in MR beyond technical saturation (B_s) in the whole range of temperatures investigated.

As noted in Section 3.1.1, for the as-quenched amorphous $Fe_{63.5}Cr_{10}Cu_1Nb_3Si_{13.5}B_9$ alloy no measurable room-temperature MR could be detected up to B=0.2 T for either the TMR or the LMR components within an accuracy of at least 0.01%. This is due to the fact that at 300 K the as-quenched amorphous state is not ferromagnetic but paramagnetic and the narrow field range did not allow us to reveal a quadratic dependence of MR on B, if there is such a component at all, in the paramagnetic state for this amorphous alloy.

It should also be mentioned that if there is an AMR component whether positive or negative, then, beyond technical saturation we should also expect an approximately linear weak decrease in the observed MR with increase in magnetic field [23], [24] and [25]. This is due to the fact that for $B>B_s$ an increasing magnetic field can induce an increase in the magnetization against thermal demagnetization (so-called paraprocess [24]). This field-induced increase in magnetic ordering results in a decrease of that component of the resistivity, which is due to the magnetic disorder, i.e., the total resistivity decreases. However, if the Curie point of that particular phase, which gives rise to the AMR effect (ascribed here to the Fe–Si nanograins with T_c of around 900 K [21]), is much higher than the temperature of the MR measurement, the magnetization is almost completely saturated and, therefore, the resistivity decrease with increase in magnetic field is extremely small. In fact, for the present nanocrystallized alloy we could not identify such a component since the MR was found to increase rather than decrease with magnetic field beyond technical saturation (see Figs. 1b, 2b and 3b).

As described in Section 3.1.2, the FM–PM transition of the residual amorphous matrix in the nanocrystallized state is around 200 K and, therefore, the MR data presented in Figs. 1–3 were obtained in the vicinity of the Curie point (T_c). It was also noted in Section 3.1.1 that the observed field dependence of MR in the high-field region is very reminiscent of the behaviour of that of disordered weak itinerant ferromagnets around the FM–PM transition. We may therefore attempt to analyse the high-field MR data along the same line as performed by Srinivas et al. [30] for an amorphous $Fe_{90}Zr_{10}$ alloy up to 4.5 T magnetic fields. The Curie point (T_c) of this alloy is 227 K [30], i.e., very close to that of the residual amorphous matrix of our nanocrystallized alloy. Srinivas et al. [30] found that for T=0.881T_c and T=1.233T_c, the field dependence of the MR can be well described by a power function MR$\propto H^n$ with the exponent n being 0.56 and 0.71, respectively, for the temperature below and above T_c.

Following the work of Srinivas et al. [30], we have also tried to fit our high-field MR data for the nanocrystallized alloy to a power function and these fits are shown by thick dashed lines in Figs. 1b–3b for each measuring temperatures. The exponent n was found to be 0.80 (LMR), 0.77 (TMR) for T=200 K, 0.41 (LMR), 0.77 (TMR) for T=250 K and 1.18 (LMR, TMR) for T=300 K. For the two lowest temperatures (200 and 250 K), these data compare well with those of Srinivas et al. [30]. However, our exponent value is higher than 1 for T=300 K and, being definitely above the Curie point of the residual amorphous matrix, this may already indicate the presence of a slight quadratic contribution in the high magnetic fields we used.

5. Summary

The magnetoresistance behaviour was investigated for a nanocrystallized $Fe_{63.5}Cr_{10}Nb_3Cu_1Si_{13.5}B_9$ alloy in the vicinity (200, 250 and 300 K) of the Curie point of the residual amorphous matrix in magnetic fields up to 12 T. The initial decrease in the resistivity for magnetic fields below about 0.1 T could be interpreted as arising from a GMR effect due to spin-dependent scattering of conduction electrons along their path between two Fe–Si nanograins via the non-magnetic matrix. For larger fields, the GMR saturated and a slightly nonlinear increase in the MR with B was observed, which could be ascribed to the contribution

by the residual amorphous matrix. By measuring separately the longitudinal and transverse MR contributions, it could be established that the AMR is negative in this nanocrystalline alloy for all fields and temperatures investigated. From MR data obtained on melt-quenched $Fe_{100-x}Si_x$ solid solutions with x=15, 18, 20, 25 and 28, this latter component could be identified as originating from the negative AMR of the Fe–Si nanograins, which exhibit the $D0_3$ structure.

Acknowledgments

This work was supported by the Hungarian Scientific Research Fund (OTKA) through Grant T 038383 as well as by the Hungarian–Spanish Bilateral Cooperation through Grant TéT E-21/04, moreover by the Spanish Government and EU FEDER (Project MAT 2007-65227) and the PAI of the Regional Government of Andalucía (Project P06-FQM-01823). The authors thank Dr. A. Rodriguez Pierna (E.U.I.T.I. of San Sebastian, University of the Basque Country, Spain) for kindly providing the original amorphous $Fe_{63.5}Cr_{10}Nb_3Cu_1Si_{13.5}B_9$ alloy ribbon. M.C. is grateful to the European Commission for financial support under a Marie Curie Intra-European Fellowship for Career Development.

References

1. Y. Yoshizawa, S. Oguma, K. Yamauchi

J. Appl. Phys., 64 (1988), p. 6044

G. Herzer

IEEE Trans. Magn., 25 (1989), p. 3327

2. G. Herzer

Scripta Metall. Mater, 33 (1995), p. 1741

3. D. Kechrakos, K.N. Trohidou

Phys. Rev. B, 62 (2000), p. 3941

P. Allia, M. Coisson, P. Tiberto, F. Vinai, M. Knobel, M.A. Novak, W.C. Nunes

Phys. Rev. B, 64 (2001), p. 144420

4. V. Franco, C.F. Conde, A. Conde, L.F. Kiss, D. Kaptás, T. Kemény, I. Vincze

J. Appl. Phys., 90 (2001), p. 1558

5. V. Franco, L.F. Kiss, T. Kemény, I. Vincze, C.F. Conde, A. Conde

Phys. Rev. B, 66 (2002), p. 224418

6. A.E. Berkowitz, J.R. Mitchell, M.J. Carey, A.P. Young, S. Zhang, F.E. Spada, F.T. Parker, A. Hutten, G. Thomas

Phys. Rev. Lett., 68 (1992), p. 3745

J.Q. Xiao, J.S. Jiang, C.L. Chien

Phys. Rev. Lett., 68 (1992), p. 3749

C.L. Chien

Mater. Sci. Eng. B, 31 (1995), p. 127

7. A. Garcia Prieto, M.L. Fdez-Gubieda, C. Meneghini, A. Garcia-Arribas, S. Mobilio

Phys. Rev. B, 67 (2003), p. 224415

8. K. Fukamichi, R.J. Gambino, T.R. McGuire

J. Appl. Phys., 53 (1982), p. 8254

9.- R. Roy, A.K. Majumdar

Phys. Rev. B, 31 (1985), p. 2033

10. S.N. Kaul, M. Rosenberg

Phys. Rev. B, 27 (1983), p. 5698

11. M. Olivier, J.O. Strom-Olsen, Z. Altounian

Phys. Rev. B, 35 (1987), p. 333

12. G. Chandra, A.K. Nigam, V. Srinivas, S. Prasad, S.N. Shringi, R. Krishnan, G. Rajaram

Mater. Sci. Eng. A, 99 (1988), p. 211

13. S.U. Jen, S.M. Yang

J. Appl. Phys., 62 (1987), p. 3323

14. A. Slawska-Waniewska, M. Kuzminski, M. Gutowski, H.K. Lachowicz

IEEE Trans. Magn., 29 (1993), p. 2628

15. M. Kuzminski, A. Slawska-Waniewska, H.K. Lachowicz, G. Herzer

IEEE Trans. Magn., 30 (1994), p. 533

16. N. Mitrovic

J. Magn. Magn. Mater., 262 (2003), p. 302

17. K. Suzuki, J.W. Cochrane, K. Aoki, J.M. Cadogan

J. Magn. Magn. Mater., 242-245 (2000), p. 273

18. A. Slawska-Waniewska, M. Gutowski, H.K. Lachowicz, T. Kulik, H. Matyja

Phys. Rev. B, 46 (1992), p. 14594

19. V. Franco, C.F. Conde, A. Conde

J. Magn. Magn. Mater., 203 (1999), p. 60

20. V. Franco, C.F. Conde, A. Conde, B. Varga, A. Lovas

J. Magn. Magn. Mater., 215–216 (2000), p. 404

21. L.K. Varga, F. Mazaleyrat, J. Kováč, J.M. Greneche

J. Phys.: Condens. Matter, 14 (2002), p. 1985

22. L.K. Varga, F. Mazaleyrat, J. Kováč, A. Kákay

J. Magn. Magn. Mater., 215–216 (2000), p. 121

L.K. Varga, F. Mazaleyrat, J. Kováč, A. Kákay

Mater. Sci. Eng. A, 304–306 (2001), p. 946

23. R.M. Bozorth

Ferromagnetism

Van Nostrand, New York (1951)

24. T.R. McGuire, R.I. Potter

IEEE Trans. Magn., 11 (1975), p. 1018

25. I.A. Campbell, A. Fert

Transport properties of ferromagnets

E.P. Wohlfarth (Ed.), Ferromagnetic Materials, vol. 3North-Holland, Amsterdam (1982) Chapter 9

26. D. Kepaptsoglu, K. Efthimiadis, P. Svec, E. Hristoforou

J. Magn. Magn. Mater, 304 (2006)e583 (2006)

27. Y. Shimada, H. Kojima

J. Appl. Phys., 49 (1978), p. 932

28. S. Giron, F. Briones, J.L. Vincent

Philos. Mag. B, 56 (1987), p. 449

29. Y. Shirakawa, Sci. Rep. Tohoku Imp. University (Sendai) 27, 255 (1939). The longitudinal MR data were measured at *H*=.15 at various temperatures from 78 K to 673 K as a function of the Si-content from 0 to 33 at.% (Fe_2Si compound). Some results are reproduced in Ref. 23 (see Fig. 16–18 on p. 759).

30. V. Srinivas, A. Perumal, A.K. Nigam, G. Chandra, A.E. George, R.A. Dunlap

Phys. Rev. B, 68 (2003), p. 104425

31. S.N. Kaul

J. Phys. F, 7 (1977), p. 2091

32. N.W. Ashcroft, N.D. Mermin

Solid State Physics

Saunders College, Philadelphia, PA, USA (1976) and Holt-Saunders Japan, Ltd., Tokyo, 1981

33. R.C. O'Handley

Modern Magnetic Materials: Principles and Applications

Wiley-Interscience, New York (2000)

34. I.A. Campbell, A. Fert, O. Jaoul

J. Phys. C, 3 (1970), p. S95

35. P. Muth, V. Christoph

J. Phys. F, 11 (1981), p. 2119

36. A. Vernes, H. Ebert, J. Banhart

Phys. Rev. B, 68 (2003), p. 134404

37. H.C. van Elst, Physica 25, 708 (1959)

38. F.C. Schwerer, J. Silcox

Phys. Rev. B, 1 (1970), p. 239

39. P. Muth, W. Heimke

Phys. Status Solidi (a), 126 (1991), p. K69

40. V.L. Moruzzi, J.F. Janak, A.R. Williams

Calculated Electronic Properties of Metals

Pergamon Press, New York (1978)

41. K.B. Hathaway, H.J.F. Jansen, A.J. Freeman

Phys. Rev. B, 31 (1985), p. 7603

42. E.G. Moroni, W. Wolf, J. Hafner, R. Podloucky

Phys. Rev. B, 59 (1999), p. 12860

43. J. Kudrnovsky, N.E. Christensen, O.K. Andersen

Phys. Rev. B, 43 (1991), p. 5924

44. N.I. Kulikov, D. Fristot, J. Hugel, A.V. Postnikov

Phys. Rev. B, 66 (2002), p. 014206

45. J. Banhart, H. Ebert, A. Vernes

Phys. Rev. B, 56 (1997), p. 10165

Table 1. Saturation values of the MR contributions for the nanocrystallized $Fe_{63.5}Cr_{10}Nb_3Cu_1Si_{13.5}B_9$ alloy: saturation field (B_s), anisotropic magnetoresistance (AMR), average saturation giant magnetoresistance component (GMR_s), LMR_s and TMR_s components of the Fe–Si nanograins. The errors of the magnitude of the GMR and the AMR which were estimated along the lines as given in the text are 30% and 50%, respectively.

Temperature (K)	**B_s (T)**	**AMR (%)**	**GMR_s (%)**	**LMR_s (Fe–Si) (%)**	**TMR_s (Fe–Si) (%)**
200	0.01	−0.004	−0.005	−0.003	0.0015
250	0.10	−0.010	−0.005	−0.007	0.0035
300	0.25	−0.015	−0.008	−0.010	0.005

Table 2. AMR magnitude, high-field slope of the MR curves, LMR and TMR values (at 0.8 T), field value B_{min}, where the TMR component has a minimum value at low fields and value of the TMR at the minimum for the rapidly quenched $Fe_{100-x}Si_x$ alloys with the $D0_3$ structure.

Si content (at%)	AMR (%)	High-field MR slope (%/T)	LMR at 0.8 T (%)	TMR at 0.8 T (%)	B_{min} (mT)	TMR_{min} (%)
18	−0.19	−0.05(2)	−0.19	0	0.04	−0.025
20	−0.20	−0.07	−0.22	−0.02	0.03	−0.015
25	−0.50	−0.21	−0.53	−0.03	0.01	−0.020
28	−0.32	−0.17	−0.36	−0.04	0.015	−0.015

Figure captions

Figure 1. (a) Experimental data (solid lines) for the longitudinal (LMR) and transverse (TMR) magnetoresistance of the nanocrystallized $Fe_{63.5}Cr_{10}Nb_3Si_{13.5}B_9Cu_1$ alloy measured at T=300 K in low magnetic fields (up to B=0.5 T). (b) Experimental data (solid lines) for the longitudinal (LMR) and transverse (TMR) magnetoresistance of the nanocrystallized $Fe_{63.5}Cr_{10}Nb_3Si_{13.5}B_9Cu_1$ alloy measured at T=300 K in magnetic fields up to B=12 T (thin solid lines) with the low-field data from (a) indicated with thick solid lines. In (b), the thick dashed lines show the fits of the data to the expression $\Delta R/R \propto H^n$. The fitted values of n are provided in Section 4.3.

Figure 2. The same as Fig. 1 but for T=250 K.

Figure 3. The same as Fig. 1 but for T=200 K.

Figure 4. Temperature dependence of the real (black squares) and imaginary (red dots) components of the a.c. susceptibility (χ_{ac}) for the $Fe_{63.5}Cr_{10}Cu_1Nb_3Si_{13.5}B_9$ alloy after nanocrystallization under optimum heat-treatment conditions (1 h for 825 K). (For interpretation of the references to colour in this figure legend, the reader is referred to the web version of this article.)

Figure 5. Room-temperature longitudinal (LMR) and transverse (TMR) magnetoresistance curves of a rapidly quenched $Fe_{80}Si_{20}$ alloy ribbon with the $D0_3$ structure in magnetic fields up to (a) B=0.8 T (black solid squares and triangles) and (b) 0.15 T (red circles and reversed open triangles). (For interpretation of the references to colour in this figure legend, the reader is referred to the web version of this article.)

Figure 1

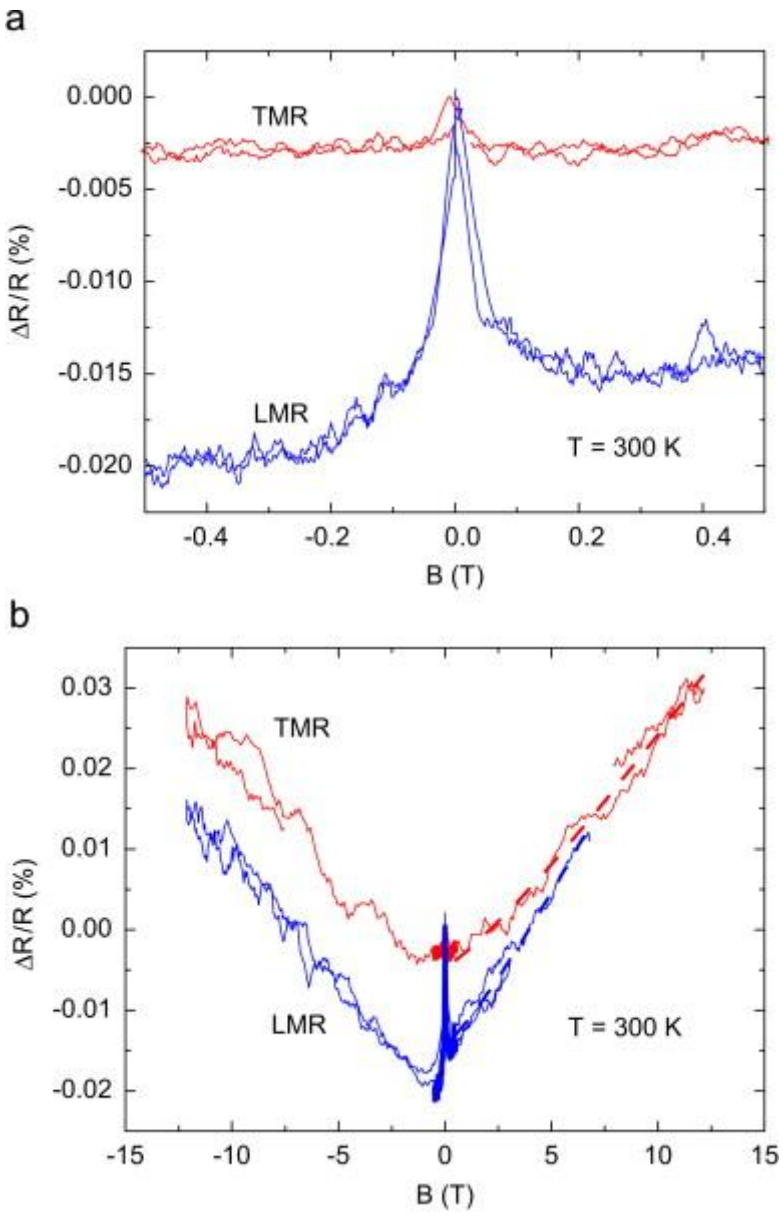
a
0.000
-0.005
-0.010
-0.015
-0.020
ΔR/R (%)
TMR
LMR
T = 300 K
-0.4
-0.2
0.0
0.2
0.4
B (T)
b
0.03
0.02
0.01
0.00
-0.01
-0.02
ΔR/R (%)
TMR
LMR
T = 300 K
-15
-10
-5
0
5
10
15
B (T)

Figure 2

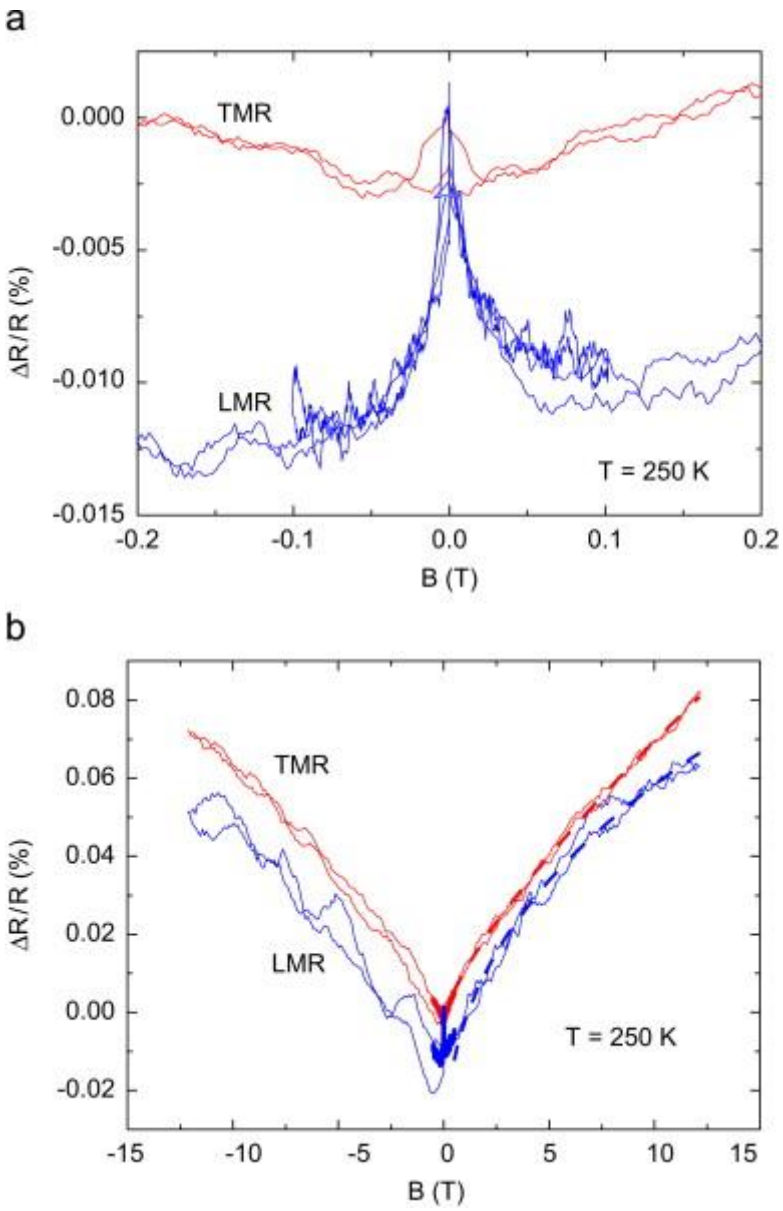
a
TMR
LMR
T = 250 K
ΔR/R (%)
B (T)
0.000
-0.005
-0.010
-0.015
-0.2
-0.1
0.0
0.1
0.2
b
TMR
LMR
T = 250 K
ΔR/R (%)
B (T)
0.08
0.06
0.04
0.02
0.00
-0.02
-15
-10
-5
0
5
10
15

Figure 3

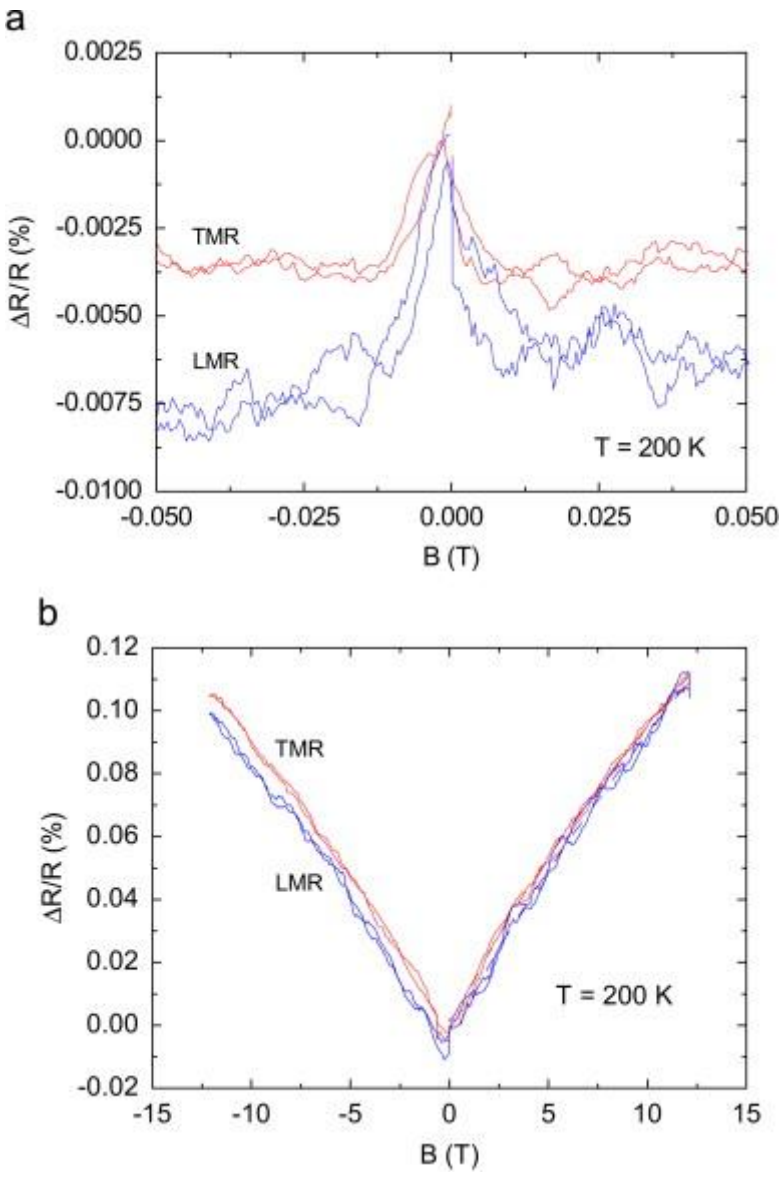
a
0.0025
0.0000
-0.0025
-0.0050
-0.0075
-0.0100
ΔR/R (%)
TMR
LMR
T = 200 K
-0.050
-0.025
0.000
0.025
0.050
B (T)
b
0.12
0.10
0.08
0.06
0.04
0.02
0.00
-0.02
ΔR/R (%)
TMR
LMR
T = 200 K
-15
-10
-5
0
5
10
15
B (T)

Figure 4

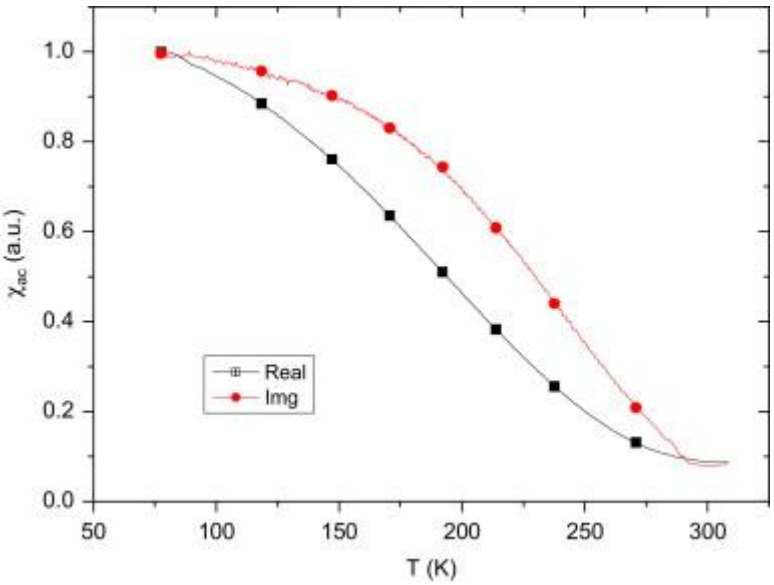

Figure 5